Permeability hysteresis from micro-channels opening during dissolution/reprecipitation cycle

Martin Lesueur[1], Thomas Poulet[2], Manolis Veveakis[1]

[1]Civil and Environmental Engineering, Duke University, Durham, NC 27708-0287, USA
[2]CSIRO Mineral Resources, 26 Dick Perry Avenue, Kensington, WA 6151, Australia

Key Points:

- Irregular permeability response from chemical porosity cycle stems from micro-channels opening and closing
- Dynamic modelling is needed to model history-dependent permeability hysteresis occurring during chemical porosity cycle
- Heterogeneous, channelised rocks display stronger deviation from porosity-permeability power law and hysteresis than homogeneous rocks

Corresponding author: Martin Lesueur, `martin.lesueur@duke.edu`

Abstract

Permeability is a critical parameter for geological resources characterisation. Its evolution with respect to porosity is particularly interesting and many research initiatives focus on deriving such relationships, to understand some hydraulic impacts of microstructure alteration. Permeability evolution from chemical reactions for instance can become complex as flow channels may open during rock dissolution. In this contribution, we show that this phenomenon can lead to irregular porosity-permeability curves and permeability hysteresis after reprecipitation. Current approaches describing permeability as a simple function of porosity can therefore not capture this behaviour and we advocate instead the use of dynamic modelling for such scenarios. We demonstrate our approach by modelling a dissolution/precipitation cycle for a unit cell pore channel and quantify the process at larger scale on three different rock samples, whose microstructures are reconstructed from segmented micro-Computerised Tomography scans.

Plain Language Summary

The ability for fluid to flow through porous rocks is quantified by the concept of permeability. This critical parameter is extensively used in geophysics and its evolution monitored with respect to porosity, the proportion of pore space volume within rocks. Porosity-permeability relationships are commonly used to obtain permeability – which is otherwise more difficult to assess – from a more tractable porosity evolution. When chemical reactions erode the rock, we show that permeability can evolve in an irregular manner as flow channels open at the pore scale. We also show that after a cycle of dissolution and reprecipitation, leading the porosity back to its original value, the permeability can actually have a different value from the initial state. This phenomenon, called permeability hysteresis, had not been explained before and here we demonstrate how it works conceptually, before showing its presence, through numerical simulation, on three different rock samples. These results are important as they show that permeability hysteresis cannot be neglected. Future modelling studies should consider this process, especially in fields like geothermal energy or carbon sequestration.

1 Introduction

Due to the importance of modelling fluid flow in the subsurface for multiple applications such as petroleum engineering, geothermal energy or carbon sequestration, rock permeability is recognised as a critical parameter to characterise. Its experimental measure, however, remains time-consuming and sometimes impractical when samples are too fragile to be processed through core flooding experiments (Ahmed et al., 1991). As such, permeability is increasingly more simulated numerically using Digital Rock Physics (Andrä et al., 2013; C. H. Arns et al., 2005), based on micro-Computerised Tomography scans of the rock samples. Its computation is mainly linked to the microstructure geometry of the porous medium and it was shown early on to depend on tortuosity (Carman, 1937). More recently, the convenience of characterising microstructure from image analysis led to the rapid development of the research field focusing on relationships between the microstructure and permeability (e.g. Bosl et al., 1998; Fauzi et al., 2002). Among the numerous parameters existing to characterise a microstructure in a porous rock, the most commonly used are the Minkowski functionals (Steele, 2007; C. Arns, 2009; Armstrong et al., 2018), including porosity, surface area, integral mean curvature and total curvature. Since porosity was historically the first identified and remains the simplest to measure, the relationship between porosity and permeability holds a particularly strong interest in research. Many analytical or empirical equations have been developed (see review from Ma, 2015) to link porosity and permeability for various types of rocks and the Kozeny-Carman relationship (Carman, 1937) is arguably the most famous one.

Those relationships were initially created to assess permeability for a distribution of porosity values. Unsurprisingly, they rapidly became used as well to compute permeability evolution from the more tractable porosity variation, for instance due to mechanical deformation (Ghabezloo et al., 2009) or, resulting in an even larger source of porosity variation, due to chemical reactions, through alteration, dissolution or precipitation (see review from Hommel et al., 2018). Such processes have more complex effects than mechanical deformation on the microstructure, however, and when we analyse chemical deformations of the medium at the micro-scale, we can even observe that the influence on fluid flow can sometimes be more discrete than continuous. Indeed, the dissolution of grains contacts or thin wall sections of the skeleton results in the creation of new channels that instantly divert fluid flow (Noiriel, 2004; Menke et al., 2014; Miller et al., 2017) and during precipitation, the opposite event of channel closure (Crandell et al., 2012). These phenomena certainly affect the permeability evolution in a non-obvious manner and no porosity-permeability relationship currently captures, to our knowledge, such complex and history-dependent processes.

In this contribution we evaluate how discrete events at the pore-scale, distributed over the entire microstructure, influence the behaviour of the Representative Elementary Volume (REV). We demonstrate how the opening and closing of micro-channels cannot necessarily be captured by history-independent relationships between microstructure and permeability and we advocate instead the use of dynamic modelling of permeability evolution by simulating explicitly the dissolution/precipitation path (e.g. Lesueur et al., 2020). We start by exposing this phenomenon for a synthetic microstructure in Sec. 2 in order to model the irreversible behaviour of the system. We then study in Sec. 3 the importance of the phenomenon on real rock microstructures.

2 Channel creation with dissolution and resulting hysteresis after re-precipitation

We start our investigation at the microstructural level of a porous rock to illustrate the phenomenon responsible for flow discontinuities during a cycle of dissolution and precipitation. We select two synthetic 2D configurations of tortuous pore throats, referred to α, our reference, and β, prone to the opening of a new flow channel, shown in Fig. 1a&d respectively. We consider the material to be chemically homogeneous and the flow to be slow enough that the dissolution is independent of the flow velocity. Under those assumptions, the dissolution happens homogeneously at the pore-grain boundary and the dissolution and precipitation stages can be simulated geometrically, using the erosion algorithm introduced by Lesueur et al. (2020). Both channels are subjected to the same cycle of dissolution and then equivalent precipitation. The dissolution is pushed enough to dissolve the matrix structure separating the flow channel of configuration β, as seen in Fig. 1e, but not sufficiently to affect configuration α the same way (see Fig. 1b). From those eroded geometries, a phase of precipitation is then applied, leading to the final states shown in Fig. 1c&f. We observe that the microstructure does revert to its initial state for one configuration only (β) but not for the other (α).

The corresponding evolutions of permeability can be computed by simulating a pressure driven Stokes flow in the channels, expressed as

$$-\mu\nabla^2\vec{v_f} + \nabla p_f = 0, \tag{1}$$
$$-\nabla \cdot \vec{v_f} = 0, \tag{2}$$

where $\vec{v_f}$ denotes the fluid velocity, p_f the pore pressure and μ the viscosity. The system of equations is solved using the Finite Element flow simulator introduced by Lesueur et al. (2017). No-slip boundary conditions are imposed at the pore-grain boundary. A pressure gradient Δp_f over the distance L_{ref} is simulated with a pressure inlet on one face and zero pressure on the opposite face. The permeability k in a selected direction

given by the normal unit vector $\vec{n}$ can then be calculated at each step of the dissolution/precipitation cycle using the formula introduced by Lesueur et al. (2017):

$$k = \mu \; L_{ref} \frac{\phi \; \vec{v_f} \cdot \vec{n}}{\Delta p_f}, \qquad (3)$$

where ϕ denotes the porosity. Since the initial structure selected is a single tortuous channel, it is expected to respect closely Poiseuille's law, in 2D, with the flow rate Q expressed for a channel of constant diameter D as

$$Q = -\frac{D^3}{12\mu}\frac{\Delta p_f}{L}, \qquad (4)$$

with L the length of the tortuous path. We can recognize here Darcy's Law, $Q = -\frac{k}{\mu}\frac{\Delta p_f}{L}$, and therefore identify the typical cubic evolution of the permeability for a widening Poiseuille channel.

The permeability evolutions resulting from the chemical cycle for both configurations are plotted in Fig. 2 and show clearly the difference between the two scenarios. Both curves, for scenarios α and β, start at the same value of porosity ($\approx 0.11\%$) and permeability (normalised to 1). They initially follow closely the expected cubic law, since the porosity is directly linked to the diameter of the channel, with the small discrepancy explained by the corner effects, where the channel diameter is not kept constant. Note that the step graph aspect of the curves comes from the fact that the erosion algorithm erodes one layer at a time and is therefore directly dependent of the mesh resolution.

We can observe that during the dissolution phase, when the porosity reaches a value of $\approx 18\%$, the permeability for scenario β jumps to a higher value by one order of magnitude. This corresponds to the configuration in Fig. 1b, where the erosion has connected the two horizontal channels parallel to each other. The discontinuous increase of permeability reflects the sudden drop of the flow path length at this specific moment. Upon further dissolution, the permeability follows a higher Poiseuille law since the tortuosity is now smaller (similarly observed by Head & Vanorio, 2016), noting that the fit is still imperfect as the diameter remains non-constant and some porosity does not contribute directly to the flow. Comparatively, the permeability evolution for configuration α remains on its initial cubic fit.

Once the porosity reaches 0.3, the dissolution process is stopped and a precipitation phase is then simulated. Interestingly, during this precipitation stage the initial channel separation of Fig. 1d cannot be recreated and upon full precipitation the newly open channel due to dissolution remains open, see Fig. 1f. This corresponds on Fig. 2 to the permeability curve of configuration β staying on the same (higher) trajectory as at the end of the dissolution. It results ultimately in a permeability hysteresis phenomenon, with the final permeability value of configuration β still one order of magnitude higher compared to the initial state, when the porosity has come back to nearly the same value ($\approx 0.11\%$). By comparison, the permeability for configuration α came back to its exact initial value.

Similarly, this study could be extended to investigate the opposite effect of microchannel closure when starting the porosity cycle with precipitation, observed on backscattered electron images (Crandell et al., 2012). A similar hysteresis is expected, as shown for example by Lesueur et al. (2020) where the permeability deviates from the Kozeny-Carman equation during precipitation.

Admittedly, this dramatic effect of permeability hysteresis was obtained on a synthetic 2D configuration. It results, however, from the creation of new channels upon dissolution, which have been documented in real rocks (Noiriel, 2004; Menke et al., 2014; Miller et al., 2017). The next step consists therefore in applying the same virtual dissolution/precipitation to realistic 3D configurations to test whether such a discontinuity of permeability evolution or permeability hysteresis could really be expected.
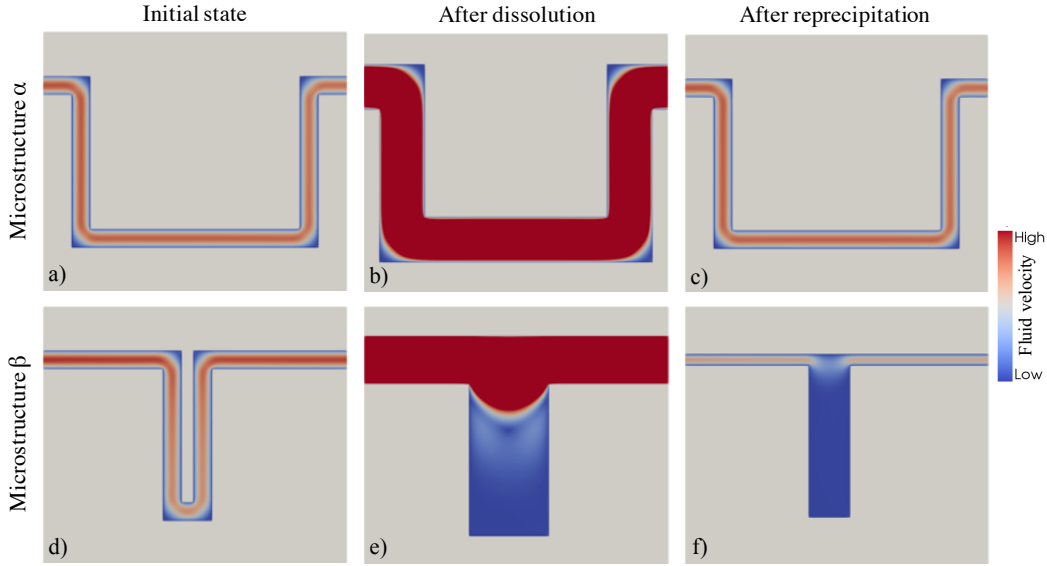
Figure 1. Evolution of fluid velocity magnitude for two synthetic microstructures (α on top and β at the bottom) during an imposed porosity cycle, showing from left to right the initial states, peak dissolution and final reprecipitation.
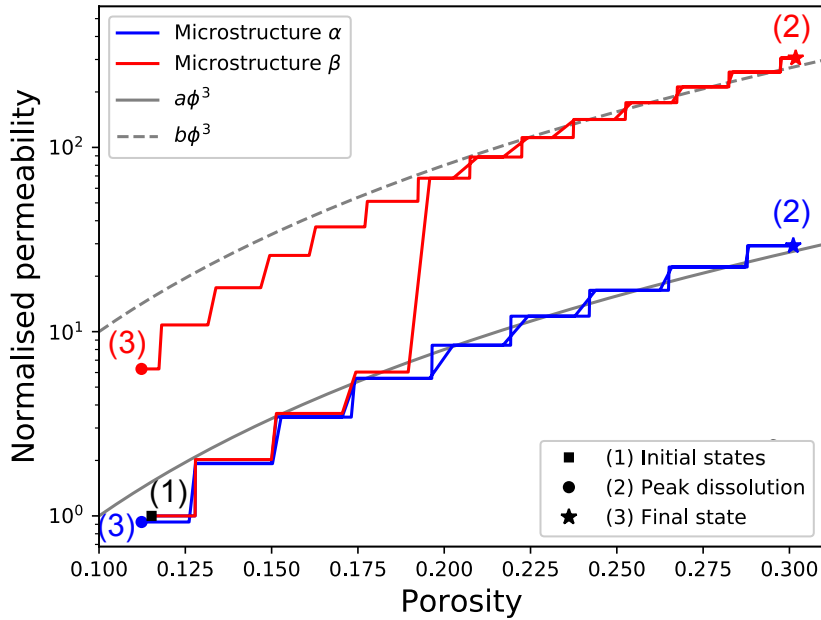
Figure 2. Evolution of permeability of the two different microstructures, α (in blue) and β (in red), from Fig 1 with respect to porosity during a cycle of imposed dissolution and reprecipitation. Permeability values are normalised with the respective values at the initial state, so both curves start therefore from the same initial state (Fig. 1a&d), marked with a square (1). The (distinct) states after dissolution (Fig. 1b&e) are marked with stars (2) and the final states, after reprecipitation (Fig. 1c&f), with squares (3). Two fitting power law trends are shown in grey (a=1000 and b=10000).

3 Analysis on real microstructures

In this section we subject various digital rock microstructures, reconstructed from segmented micro-Computerised Tomography scans following the methodology of (Lesueur et al., 2017), to a virtual cycle of dissolution/precipitation and compute the corresponding permeability evolutions, shown on Fig. 3. We select three rock samples that have different levels of heterogeneity.

The first sample, whose response is plotted in blue on Fig. 3, is the LV60A sandpack (Imperial College Consortium On Pore-Scale Modelling, 2014b). As a synthetic rock, it has a very homogeneous granular structure, close to a Random Close Packing (RCP), as highlighted by its porosity of 37% compared to 36.5% for the RCP. We select a cubic sample size of 1.2 mm to start at REV size (Mostaghimi et al., 2012; Lesueur et al., 2017). As seen in Fig. 3, the permeability response from a porosity cycle does not exhibit much hysteresis on a logarithmic scale, but still varies by $\approx$21%. Following (Hommel et al., 2018), we can fit a porosity-permeability power law ax^b with an exponent $b = 4.3$ and see that the structure globally follows the fitting law during the whole cycle. Note that the parameter a was fitted to fall exactly on the initial state for all cases.

The second sample, corresponding to the green curve in Fig. 3, is the S1 sandstone (Imperial College Consortium On Pore-Scale Modelling, 2014c). It also has a granular and rather homogeneous structure but it is a natural material so it is more heterogeneous compared to the previous sandpack. Its initial porosity is also lower ($\approx$14%). We select a cubic sample of size 2.2 mm, above the REV size (Mostaghimi et al., 2012). Despite a small hysteresis phenomenon visible during the cycle, the final value of permeability ends up nearly identical to the initial one, with less than 3% difference. The permeability evolution follows overall a power law relationship with an exponent of 3.

The third sample, corresponding to the red curve in Fig. 3, is the C1 carbonate (Imperial College Consortium On Pore-Scale Modelling, 2014a). Due to the geometry of the skeleton, the flow is focused in a few channels as observed in Fig. 4. (Mostaghimi et al., 2012) showed that this structure does not actually reach any REV, which can be a common feature for carbonate rocks (see Liu et al., 2014, for another example). Still, the cubic sample selected, of size 0.7 mm, remains a Statistical REV (Zhang et al., 2000) as we can see the flow composed by a sufficient number of channels in Fig. 4. This structure is therefore quite heterogeneous. Past a porosity of 36% during the dissolution stage of the porosity cycle, we observe a clear deviation from the power law of exponent 2.5, that was originally fitting nicely the first stage of dissolution. This deviation clearly indicates the opening of new channels and is visualised in Fig. 4. Upon further dissolution, the structure does not seem to stabilise on any power law trajectory as more channels open up. The precipitation path is also quite irregular and does not follow any power law. At the final stage of precipitation, the hysteresis is important, with $\approx$110% increase in permeability compared to the initial state. Indeed, the microstructure of the reprecipitated carbonate is quite different from the initial one, visualised in Fig. 4, with some channels having closed and some new ones having appeared. Particularly, the new channels that have opened during dissolution and remained open after reprecipitation could explain the higher permeability in the final state.

4 Discussion

The results of Sec. 2 and 3 show that irregularities in the porosity-permeability responses from a cycle of dissolution/precipitation originate from the opening and closing of micro flow channels, observed for example by Noiriel (2004); Crandell et al. (2012). Such discrete events at the micro-scale trigger flow discontinuities (see Sec. 2) and it is the accumulation of those events that influences how marked the irregularity in the permeability response will appear at the larger scale (see Sec. 3). Due to the variability in
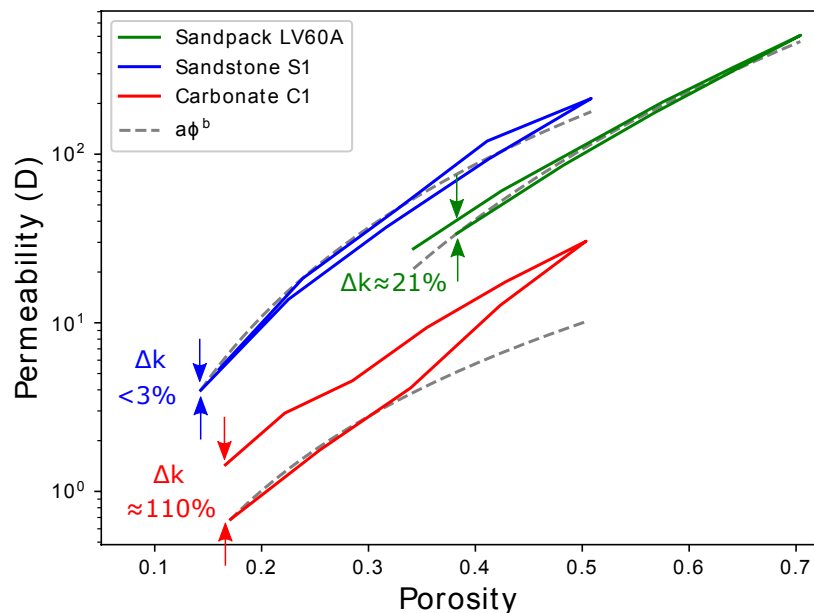
Figure 3. Evolution of permeability of three different rock samples with respect to porosity during a virtual cycle of dissolution/reprecipitation, along with power law fitting curves. The numerical results for the sandpack LV60A are shown in green (fitted with power law exponent $b = 4.3$), those for the sandstone S1 in blue (exponent $b = 3$) and those for the carbonate C1 in red (exponent $b = 2.5$).
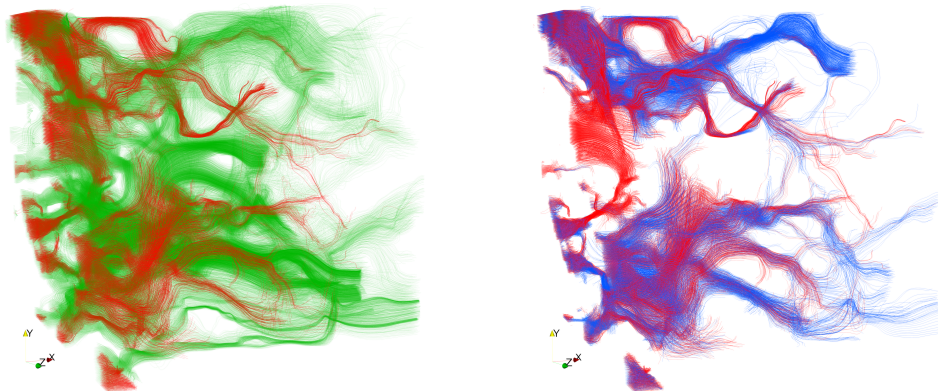
Figure 4. Visualisation of streamlines through the chemically altered carbonate C1 sample, of size 0.7 mm. The streamlines for the initial state, at 17% porosity, are represented in red and can be compared with those in green (left hand side) at peak dissolution (50.3% porosity) and in blue (right hand side) for the final state after reprecipitation (16.6% porosity). Videos of the full orbital view of the two figures can be found in Supplementary Information.

the distribution of material and geometrical properties of the rock, micro events of channel creation and closure occur in a staggered and desynchronised manner. Compared to the discontinuous nature of a single event (see Sec. 2), the permeability response at the larger scale displays therefore irregularity in a smoother manner (see Sec. 3). Also, heterogeneous and channelised samples like the carbonate C1 display a more drastic permeability deviation from the power law trend as channelised flow tends to be closer to the unit cell behaviour considered in Sec. 2. This result is well aligned with observations from the experiments of Menke et al. (2014) displaying drastic permeability increase in a channelised sample of limestone, when a dissolution pathway connects. These results could be linked to observations at the micro-scale, like the ones from Noiriel (2004).

The irregular permeability response to a porosity cycle can lead to a phenomenon of hysteresis, for which different permeability values can exist at the same porosity for one sample. This phenomenon can be explained by the fact that opening or closure of flow micro-channels mark irreversible permeability transitions and it cannot be reverted simply through an inversion of the chemical process. It is then the accumulation of those events that will determine the magnitude of the hysteresis, which is then directly dependent on the geometry of the microstructure of the rock. While it can reach non-negligible values for the carbonate C1 for example, there is also the possibility for the dissolution/precipitation loop to even close back on itself, as for the case of the sandstone S1. The permeability response of a chemical porosity variation is clearly history-dependent and porosity-permeability relationships used in such a context should therefore account for it accordingly.

Sec. 2 showed how the opening of one flow channel can influence the permeability of the porous medium and it is interesting to check which measurable parameters of the microstructure, if any, control this behaviour. The α and β configurations displayed a radically different permeability evolution during a dissolution/precipitation cycle. When subjected to the same imposed porosity evolution, configuration β did not open any new channel and the porosity cycle was completely reversible, whereas configuration α led to a marked permeability hysteresis. Yet, both structures are actually extremely similar in the sense that, from an homogenised perspective, their microstructures could be qualified of identical. They have indeed many indistinguishable characteristic properties, including the same porosity, tortuosity, specific surface area, curvature and permeability. This indicates that the conventional parameters used to characterise microstructure are currently not adapted to quantify the permeability hysteresis phenomenon described here. Yet, this phenomenon is non-negligible (see Fig. 3) and should be accounted for, which means that a new measurable characteristic of the microstructure needs to be identified. The only difference between the α and β configurations comes from the length of the gap between the parallel channels, see Fig. 1a compared to Fig. 1d. For real rocks, as tested in Sec. 3, this would correspond to the thickness of walls between pores. By characterising such a controlling parameter, the phenomenon of permeability hysteresis could potentially be modelled through analytical relationships.

The results showed in this contribution were based on the assumptions of homogeneous rocks and slow enough chemical reactions (low Damköhler numbers), allowing a purely geometrical simulation of the dissolution and precipitation phases. Dissolution-precipitation reactions are obviously more complex locally (Renard et al., 2019) and more advanced chemical simulations of those phenomena can be modelled (e.g. Kang et al., 2003; Kondratiuk et al., 2015; Nunes et al., 2016) to provide results in different contexts. However, the same fundamental processes of micro-channel creation and closure still occurs (see e.g. Miller et al., 2017) and we expect therefore similar results qualitatively. We would even expect more pronounced permeability hysteresis under higher reaction rates, both from this study and also the fact that hysteresis has been observed even without the opening of channels (Kang et al., 2003).

5 Conclusions

In this contribution we showed the effect on permeability of the opening of new flow channels at the pore scale during rock dissolution. We demonstrated for a unique pore throat how such a discrete event can result in a permeability jump and hysteresis after a reprecipitation cycle. Localized jumps at the micro-scale are smoothed out at the scale of the REV and the accumulation of those events on the dissolution path can result in a clear deviation of the permeability from a power law with respect to porosity. The resulting hysteresis was shown to be more pronounced for more channelized and heterogeneous samples and we showed that the conventional parameters characterising the microstructure are not the controlling parameters for this permeability hysteresis phenomenon. The history-dependent nature of chemical porosity evolution shows that static porosity-permeability relationships are not well suited for this kind of modelling and we advocate instead the use of dynamic modelling that takes directly into account the dissolution/precipitation path (e.g. Lesueur et al., 2020).

References

Ahmed, U., Crary, S. F., & Coates, G. R. (1991). Permeability estimation. The various sources and their interrelationships. *Journal of Petroleum Technology*, *43*(5), 578–587. doi: 10.2118/19604-PA

Andrä, H., Combaret, N., Dvorkin, J., Glatt, E., Han, J., Kabel, M., ... Zhan, X. (2013, jan). Digital rock physics benchmarks—part II: Computing effective properties. *Computers & Geosciences*, *50*, 33–43. doi: 10.1016/j.cageo.2012.09.008

Armstrong, R. T., McClure, J. E., Robins, V., Liu, Z., Arns, C. H., Schlüter, S., & Berg, S. (2018, nov). Porous media characterization using minkowski functionals: Theories, applications and future directions. *Transport in Porous Media*, *130*(1), 305–335. doi: 10.1007/s11242-018-1201-4

Arns, C. (2009). *Structure-property relationships from digital images*. VDM Verlag.

Arns, C. H., Bauget, F., Limaye, A., Sakellariou, A., Senden, T., Sheppard, A., ... Knackstedt, M. A. (2005, dec). Pore scale characterization of carbonates using x-ray microtomography. *SPE Journal*, *10*(04), 475–484. doi: 10.2118/90368-pa

Bosl, W. J., Dvorkin, J., & Nur, A. (1998, may). A study of porosity and permeability using a lattice boltzmann simulation. *Geophysical Research Letters*, *25*(9), 1475–1478. doi: 10.1029/98gl00859

Carman, P. C. (1937). Fluid flow through granular beds. *Trans. Inst. Chem. Eng.*, *15*, 150–166.

Crandell, L., Peters, C., Um, W., Jones, K., & Lindquist, W. (2012, apr). Changes in the pore network structure of hanford sediment after reaction with caustic tank wastes. *Journal of Contaminant Hydrology*, *131*(1-4), 89–99. doi: 10.1016/j.jconhyd.2012.02.002

Fauzi, U., Hoerdt, A., & Neubauer, F. M. (2002, apr). Influence of coordination number and percolation probability on rock permeability estimation. *Geophysical Research Letters*, *29*(8), 78–1–78–4. doi: 10.1029/2001gl013414

Ghabezloo, S., Sulem, J., & Saint-Marc, J. (2009, jun). Evaluation of a permeability–porosity relationship in a low-permeability creeping material using a single

transient test. *International Journal of Rock Mechanics and Mining Sciences*, *46*(4), 761–768. doi: 10.1016/j.ijrmms.2008.10.003

Head, D., & Vanorio, T. (2016, jul). Effects of changes in rock microstructures on permeability: 3-d printing investigation. *Geophysical Research Letters*, *43*(14), 7494–7502. doi: 10.1002/2016gl069334

Hommel, J., Coltman, E., & Class, H. (2018, may). Porosity–permeability relations for evolving pore space: A review with a focus on (bio-)geochemically altered porous media. *Transport in Porous Media*, *124*(2), 589–629. doi: 10.1007/s11242-018-1086-2

Imperial College Consortium On Pore-Scale Modelling. (2014a). *C1 carbonate.* Figshare. doi: 10.6084/m9.figshare.1189257

Imperial College Consortium On Pore-Scale Modelling. (2014b). *Lv60a sandpack.* Figshare. doi: 10.6084/m9.figshare.1153795

Imperial College Consortium On Pore-Scale Modelling. (2014c). *S1 sandstone.* Figshare. doi: 10.6084/m9.figshare.1189274.v1

Kang, Q., Zhang, D., & Chen, S. (2003, oct). Simulation of dissolution and precipitation in porous media. *Journal of Geophysical Research: Solid Earth*, *108*(B10). doi: 10.1029/2003jb002504

Kondratiuk, P., Tredak, H., Ladd, A. J. C., & Szymczak, P. (2015, apr). Synchronization of dissolution and precipitation fronts during infiltration-driven replacement in porous rocks. *Geophysical Research Letters*, *42*(7), 2244–2252. doi: 10.1002/2015gl063146

Lesueur, M., Casadiego, M. C., Veveakis, M., & Poulet, T. (2017, dec). Modelling fluid-microstructure interaction on elasto-visco-plastic digital rocks. *Geomechanics for Energy and the Environment*, *12*, 1–13. doi: 10.1016/j.gete.2017.08.001

Lesueur, M., Poulet, T., & Veveakis, M. (2020, jun). Three-scale multiphysics finite element framework (FE3) modelling fault reactivation. *Computer Methods in Applied Mechanics and Engineering*, *365*, 112988. doi: 10.1016/j.cma.2020.112988

Liu, J., Pereira, G. G., & Regenauer-Lieb, K. (2014, sep). From characterisation of pore-structures to simulations of pore-scale fluid flow and the upscaling of permeability using microtomography: A case study of heterogeneous carbonates. *Journal of Geochemical Exploration*, *144*, 84–96. doi: 10.1016/j.gexplo.2014.01.021

Ma, J. (2015, jun). Review of permeability evolution model for fractured porous media. *Journal of Rock Mechanics and Geotechnical Engineering*, *7*(3), 351–357. doi: 10.1016/j.jrmge.2014.12.003

Menke, H., Bijeljic, B., Andrew, M., & Blunt, M. J. (2014). Dynamic pore-scale imaging of reactive transport in heterogeneous carbonates at reservoir conditions. *Energy Procedia*, *63*, 5503–5511. doi: 10.1016/j.egypro.2014.11.583

Miller, K., Vanorio, T., & Keehm, Y. (2017, jun). Evolution of permeability and microstructure of tight carbonates due to numerical simulation of calcite dissolution. *Journal of Geophysical Research: Solid Earth*, *122*(6), 4460–4474. doi: 10.1002/2017jb013972

Mostaghimi, P., Blunt, M. J., & Bijeljic, B. (2012, dec). Computations of absolute permeability on micro-CT images. *Mathematical Geosciences*, *45*(1), 103–125. doi: 10.1007/s11004-012-9431-4

Noiriel, C. (2004). Investigation of porosity and permeability effects from microstructure changes during limestone dissolution. *Geophysical Research Letters*, *31*(24). doi: 10.1029/2004gl021572

Nunes, J. P. P., Blunt, M. J., & Bijeljic, B. (2016, feb). Pore-scale simulation of carbonate dissolution in micro-CT images. *Journal of Geophysical Research: Solid Earth*, *121*(2), 558–576. doi: 10.1002/2015jb012117

Renard, F., Røyne, A., & Putnis, C. V. (2019, jan). Timescales of interface-coupled

dissolution-precipitation reactions on carbonates. *Geoscience Frontiers*, *10*(1), 17–27. doi: 10.1016/j.gsf.2018.02.013

Steele, J. (2007, aug). Characterizing 3d microstructure using the minkowski functionals. *Microscopy and Microanalysis*, *13*(S02). doi: 10.1017/ s1431927607075691

Zhang, D., Zhang, R., Chen, S., & Soll, W. E. (2000, apr). Pore scale study of flow in porous media: Scale dependency, REV, and statistical REV. *Geophysical Research Letters*, *27*(8), 1195–1198. doi: 10.1029/1999gl011101